ADVANCED SENSOR RESEARCH Open Access
www.advsensorres.com

Virulent Factor-Targeted Point-of-Care Biosensor for Detection of Staphylococcus Aureus Infections

*Zahra Marvi, Yara Raphael, Dario Job, Graziele Cruzado, and Geraldine Merle**

Rapid detection of pathogenic bacteria like *Staphylococcus aureus* (*S. aureus*) is crucial for timely diagnosis and infection control. Aureolysin (Aur), an extracellular metalloprotease involved in *S. aureus* pathogenesis, is a promising biomarker. This study presents a rapid, low-cost, label-free electrochemical immunosensor for aureolysin detection using antibody-gold (Ab-Au) bioconjugates. Anti-aureolysin antibodies are immobilized on gold nanospikes via 1-Ethyl-3-(3-dimethylaminopropyl)carbodiimide / N-Hydroxysuccinimide (EDC/NHS) chemistry and screen-printed gold electrodes (SPGEs). The detection relied on changes in peak current from antigen-antibody complex formation, measured through differential pulse voltammetry (DPV). Selectivity tests confirmed the sensor's specificity for *S. aureus*, with no cross-reactivity against *Escherichia coli* or *Pseudomonas aeruginosa*. A strong linear correlation ($R^2 = 0.9739$) between peak current and logarithmic *S. aureus* concentrations is observed, with a detection limit of 5 pg·mL^{-1} in buffer and 2 Colony-forming unit (CFU) mL^{-1} in bacterial cultures. The sensor also detected *S. aureus* in biofilms, highlighting its potential for real-world use. Offering rapid detection within 1h, high sensitivity, and specificity, this immunosensor is a promising point-of-care tool for *S. aureus* detection in clinical settings. This approach greatly enhances the sensor's effectiveness in real-world clinical applications, where biofilm formation often complicates diagnosis and treatment.

1. Introduction

Staphylococcus aureus (*S. aureus*) is a Gram-positive bacterium that causes severe, invasive infections with high morbidity and mortality rates, including periprosthetic joint infection (PJI), pneumonia, nosocomial bacteremia, and foodborne infections.[1–3] Rapid and accurate detection of *S. aureus* is crucial for appropriate clinical management and infection control measures. Currently, available methods for detecting *S. aureus* include culture-based methods, molecular methods such as polymerase chain reaction (PCR),[4] matrix-assisted laser desorption/ionization time of flight mass spectrometry,[5] and enzyme-linked immunosorbent assays (ELISAs).[6] The gold standard culture-based testing method is time-consuming, often requiring between 3 days to several weeks, laborious, and necessitates technical expertise.[7] While PCR offers high sensitivity, it remains costly and is not able to distinguish between viable and nonviable bacteria.[4,8] ELISAs provide a shorter detection time (<6h) compared to the culture-based method, but they are prone to cross-contamination and exhibit poor stability, limiting their application for real-time *S. aureus* detection.[9]

Electrochemical detection has emerged as a promising alternative to traditional methods due to its rapidity, high sensitivity, reliability, and ease of miniaturization, making it an attractive solution for real-time pathogen detection.[10–16] Various electrochemical sensors have been developed for bacterial infection detection, each offering distinct advantages and limitations. Several biorecognition elements including antibodies, enzymes, and nucleic acids have been employed in these sensors, tailored to specific applications and bacterial targets. Among them, antibody-based electrochemical sensors have been applied for *S. aureus* detection.[17–19] For instance, A 2D metal-organic framewor (MOF) nanozyme-amplified electrochemical biosensor utilizing dual recognition, vancomycin, and anti-*S. aureus* antibody demonstrated sensitive and selective detection of *S. aureus* with a detection limit of 6 CFU mL^{-1}.[20] Another study, reported an electrochemical impedimetric immunosensor with silanized Indium Tin Oxide (ITO) electrodes modified by gold nanoparticles (AuNPs), for the detection of *Staphylococcus aureus* achieving a limit of detection (LOD) of 3×10^3 CFU mL^{-1}.[21] In a recent study, an immunosensor using a layer-by-layer film of chitosan and carboxylate multi-walled carbon nanotubes successfully

Z. Marvi, Y. Raphael, D. Job, G. Cruzado, G. Merle
Department of Chemical Engineering
Polytechnique Montreal
Montreal, Quebec, Canada
E-mail: geraldine.merle@polymtl.ca
G. Merle
Department of Surgery
Faculty of Medicine
McGill University
Montreal, Quebec, Canada

The ORCID identification number(s) for the author(s) of this article can be found under https://doi.org/10.1002/adsr.202400153

© 2025 The Author(s). Advanced Sensor Research published by Wiley-VCH GmbH. This is an open access article under the terms of the Creative Commons Attribution License, which permits use, distribution and reproduction in any medium, provided the original work is properly cited.

DOI: 10.1002/adsr.202400153

detected *Staphylococcus aureus* in milk samples with a limit of detection of 2.6 CFU mL^{-1}.[22]

Other studies have explored nucleic acids and aptamers for signal amplification. For example, Cai and colleagues developed an electrochemical biosensor utilizing a DNA walker and DNA nanoflowers; employing rolling circle amplification to achieve a limit of detection of 9 CFU mL^{-1} for *S. aureus*.[14] Wu et al. applied dual recognition units —a DNA walker and Pb^{2+}-specific DNA zyme— for detecting *S. aureus*, achieving a linear detection range of 10–10^7 CFU mL^{-1} with a LOD of 1 CFU mL^{-1}.[15] While these approaches have demonstrated enhanced signal sensitivity with low limits of detection, they often involve complex fabrication processes and biological preparation steps. Furthermore, immunosensors that target whole bacteria, such as *S. aureus* (≈0.5–1.5 μm in diameter), may face limitations in sensitivity.[23]

Most current studies have focused on the electrochemical detection of *S. aureus* in food products, with limited research addressing medical applications. In particular, there is a notable gap in the detection of complex conditions involving microbial biofilm formation such as PJI, where the causative bacteria tend to concentrate on the prosthesis surface, necessitating more targeted detection approaches.[24]

Gold surfaces have been widely employed as biosensing platforms owing to their superior electrical conductivity, biocompatibility, and ease of functionalization with biomolecules.[25–28] Electrochemical deposition of gold nanostructures has been a well-established method to produce high aspect ratio morphologies, such as rods, pyramids, and spikes.[29–31] Among these, Au nanospikes are particularly advantageous, offering a stable substrate for antibody immobilization and enhancing electrochemical performance. This is attributed to their dominant (111) crystal orientation, which promotes electrocatalytic activity,[32] and their high index (311) facets, which offer a high density of kinks and atomic steps, thereby increasing the number of active sites.[33,34]

While numerous approaches have been developed to improve detection sensitivity, maintaining the device architecture simplicity and cost-effectiveness of the biosensing platform is critical for widespread implementation.

In this work, we present an ultra-sensitive, label-free immunosensor for the detection of *S. aureus* through the quantification of aureolysin (Aur) for the first time. Aureolysin, a 33 KDa single-chain extracellular metalloprotease,[35] is a highly conserved virulence factor of *S. aureus* and consistently present across 96% of *S. aureus* strains examined.[36,37] It plays a pivotal role not only in the pathogenesis of *S. aureus* but also in inhibiting the complement response of the host's immune system.[38] Functionally, Aur cleaves antimicrobial peptide LL-37 and complement component C3, impairing opsonization and neutrophil-mediated clearance.[39] Moreover, it is responsible for nearly 50% of all peptidase activity in *S. aureus* cultures.[39] Aur has been identified in various *S. aureus*-associated infections, including pneumonia, skin infections, sepsis, furuncles, and atopic dermatitis, and is significantly upregulated during biofilm maturation and invasive infection stages, as observed in transcriptomic studies of *S. aureus*-induced osteomyelitis and prosthetic valve endocarditis.[36,40–42] While Aur is primarily secreted at the infection site, its role in biofilm detachment and bacterial dissemination suggests that it may enter the bloodstream as the infection progresses. Given its immunoreactive properties, elevated expression in progressive infections, and presence in diverse clinical manifestations, Aur holds promise as a biomarker for diverse clinical scenarios where *S. aureus* is implicated, particularly in biofilm-related infections. The role of Aur in stabilizing virulence factors like alpha-toxin and phenol-soluble modulins,[43,44] suggests that its presence signals a broader range of virulence, providing insight into infection severity and treatment challenges. Additionally, its identification can be further used as a target for novel therapeutic protease inhibitors and enhancing the efficacy of the current antibiotics, particularly in the context of rising antibiotic resistance.[45] To the best of our knowledge, this is the first instance of aureolysin being leveraged as a biomarker for *S. aureus* infection, paving the way for future clinical applications. **Figure 1** illustrates a potential approach for diagnosing PJI using our sensor as an example of its clinical application. Synovial fluid is the preferred diagnostic sample, as it directly reflects biofilm-associated bacterial activity and specific infection markers.[46] In advanced cases with bacterial spread, Aur may enter circulation, making blood a possible secondary diagnostic matrix.

In this study, a screen-printed gold electrode (SPGE) was modified with Au nanospikes through electrochemical deposition to increase the electrochemically active surface area, thereby amplifying the signal. The modified electrode was functionalized with a self-assembled layer of 11-Mercaptoundecanoic acid via thiol chemistry, followed by grafting of an anti-Aur antibody. The efficacy of this immunosensor was validated through the quantification of aureolysin in phosphate-buffered saline (PBS) as well as *S. aureus* in bacterial culture and biofilm. This method demonstrated a significant enhancement in electrochemical signals, with the response being directly proportional to the concentration of *S. aureus*. Additionally, the immunosensor demonstrated excellent selectivity when tested against other bacterial species.

2. Materials and Methods

2.1. Materials and Reagents

11-Mercaptoundecanoic acid (MUA), Phosphate buffer saline (PBS, 0.01 M, pH 7.4), tetra chloroauric(III) acid trihydrate ($HAuCl_4 \cdot 3H_2O$), lead(II) acetate trihydrate ($(CH_3COO)_2Pb \cdot 3\ H_2O$), bovine serum albumin (BSA), 1-ethyl-3- (3-(dimethylamine)propyl) carbodiimide (EDC), N-hydroxysuccinimide (NHS), sulfuric acid (98%), 4-morpholineethanesulfonic acid (MES), potassium ferrocyanide ($K_4[Fe(CN)_6]$, 99%), potassium ferricyanide ($K_3[Fe(CN)_6]$, 99%) were purchased from Sigma-Aldrich. Recombinant *Staphylococcus aureus* Zinc metalloproteinase aureolysin was obtained from My BioSource, and an anti-aureolysin polyclonal antibody was purchased from CUSABIO. The antibody and enzyme solutions were prepared with 0.01 M PBS. *E. coli*, *S. aureus*, and *P. aeruginosa* were provided by the chemical engineering school of Polytechnique Montreal. Luria-Bertani (LB) broth was purchased from VWR chemicals, and cellulose sheets were acquired from Biofilm. Ultrapure water (18.2 MΩ cm^{-1}) from a Milli-Q system was used for all the steps. All other chemicals were of analytical grade.

© 2025 The Author(s). Advanced Sensor Research published by Wiley-VCH GmbH

27511219, 2025, 4, Downloaded from https://advanced.onlinelibrary.wiley.com/doi/10.1002/adsr.202400153, Wiley Online Library on [23/10/2025]. See the Terms and Conditions (https://onlinelibrary.wiley.com/terms-and-conditions) on Wiley Online Library for rules of use; OA articles are governed by the applicable Creative Commons License

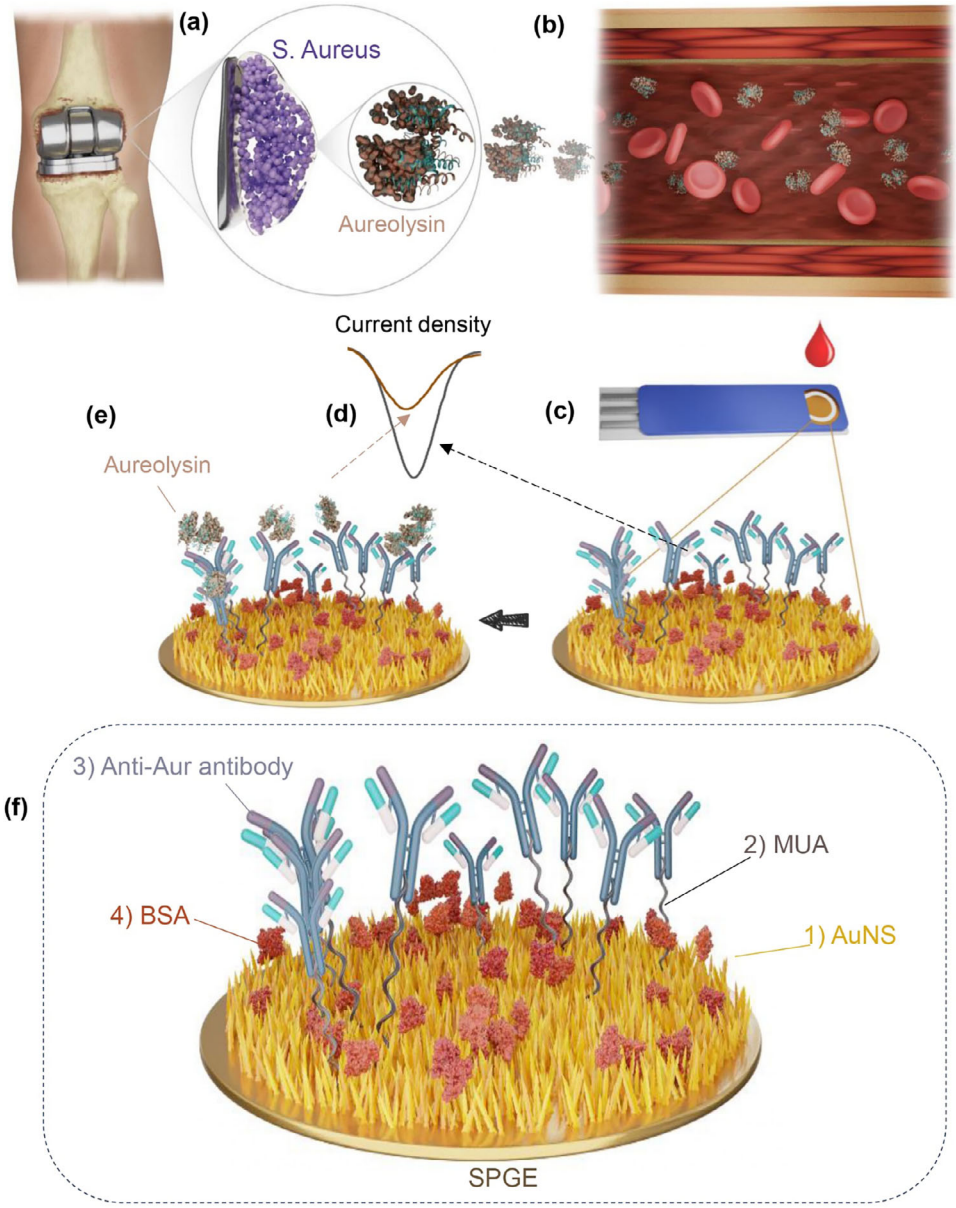

Figure 1. Schematic illustration of Aureolysin detection in PJI as a potential application. A,B) Secretion of aureolysin during PJI and its release into the bloodstream. Initially, *S. aureus* forms a biofilm on the prosthetic surface, where Aur is secreted to facilitate bacterial spread. As the infection progresses, Aur may enter the circulatory system through biofilm detachment. While synovial fluid remains the primary diagnostic sample for PJI, blood samples on the fabricated sensor may serve as an indicator of advanced infection. D) Voltametric responses before and after sample exposure on the surface of the immunosensor. E) Aureolysin specific binding to BSA-Antibody-MUA-Au nanospike-SPGE. F) Final structure of immunosensor after four-step preparation.

2.2. Aureolysin Immunosensor

The fabrication process of the immunosensor, resulting in the final structure illustrated in Figure 1f, involves four main components and is completed in four sequential steps: 1) deposition of Au nanostructures, 2) activation of the Au surface with MUA, 3) antibody immobilization, and 4) adsorption of BSA.

Au nanospikes were deposited onto the SPGE via electrochemical deposition, as described in the method reported by Plowman et al.[30] The SPGE was immersed in a solution containing Pb $(CH_3COO)_2$ (0.5 mM) and $HAuCl_4$ (6.9 mM), and a potential of 50 mV was applied for 10 min. The resulting nanospike SPGE was then scanned in an H_2SO_4 (0.1 M) solution using cyclic voltammetry (CV) over a potential range from 0.5 to 1.4 V at a scan rate of 0.5 V s^{-1}. After scanning, the electrode was thoroughly rinsed with ultra-pure water and dried for the next step.

The cleaned Au Nanospikes-SPGE was immersed in a solution of MUA (10 μM) in ethanol for 2h to form a self-assembled monolayer on the electrode surface. Subsequently, the electrode was

 © 2025 The Author(s). Advanced Sensor Research published by Wiley-VCH GmbH

27511219, 2025, 4, Downloaded from https://advanced.onlinelibrary.wiley.com/doi/10.1002/adsr.202400153, Wiley Online Library on [23/10/2025]. See the Terms and Conditions (https://onlinelibrary.wiley.com/terms-and-conditions) on Wiley Online Library for rules of use; OA articles are governed by the applicable Creative Commons License

thoroughly rinsed with ethanol and ultra-pure water and dipped in and EDC/NHS solution (400 mM/100 mM in MES, pH 6) for 1h to activate the carboxyl groups of MUA. After activation, of anti-Aur antibody (20 µL, 100 µg mL^{-1}) was drop-casted on the SPGE surface and incubated for 2h for antibody binding, followed by rinsing with PBS. A solution of BSA (1%) was subsequently used for 30 min to block non-specific interaction. All fabrication steps were performed at room temperature. The completed BSA-Antibody-MUA-Aunanospike-SPGE immunosensor was stored at 4 °C for future use.

2.3. Characterization of SPGE

The surface morphology of the modified screen-printed electrode was investigated using scanning electron microscopy (SEM, Inspect F50, FEI Company, Hillsboro, OR, USA). Electrochemical measurements were carried out with a potentiostat (Versa STAT 4, Princeton Applied Research, Oak Ridge, TN, USA) and Screen-printed gold electrodes (SPGE, ϕ = 4 mm) with Ag as reference electrode and carbon as the counter electrode (Metrohm Canada). Cyclic voltammetry was conducted in the potential range of −0.4 to 0.6 V and at the scan rate of 50 mV s^{-1}. Differential pulse voltammetry (DPV) was performed within a potential range of −0.4 to 0.4 V, using a step of 5 mV, a modulation amplitude of 50 mV, a modulation time of 0.05 s, and an interval time of 0.2 s, in a$[K_3Fe(CN)_6]/[K_4Fe(CN)_6]$ (5 mM/5 mM) solution with PBS (0.1 M) (pH 7.4).

PBS solutions (pH 7.4) of aureolysin were prepared at different concentrations of 1, 10, 40, 50, 70, and 100 pg. mL^{-1}. For each concentration, 20 µL of solution was drop casted on the surface of BSA-Antibody-MUA-Aunanospike-SPGE biosensor and incubated for 1h at room temperature. Following incubation, the electrode was rinsed with ultra-filtered water and PBS solution to remove unbound Aur and dried. Differential pulse voltammetry measurements were then performed in a solution of $[K_3Fe(CN)_6]/[K_4Fe(CN)_6]$ (5 mM/5 mM), as the redox couple, in 10 mM PBS (pH 7.4).

The sensor's specificity to *S. aureus* was investigated by comparing the response to other PJI pathogens *E. coli* and *P. aeruginosa*. For this purpose, *E. coli*, *S. aureus*, and *P. aeruginosa* were cultured in LB broth medium at 36 °C for 24 h. Cells were suspended and serially diluted to desired concentrations (1–10^8 CFU for *Staphylococcus aureus* and 10^5 CFU for *E. coli* and *P. aeruginosa*) in a suspension medium composed of nutrient broth (NB 1/500), made using ISO22196:2011 by mixing meat extract (3.0g), peptone (10.0g), and sodium chloride (5.0g) in deionized water (1.0 L)). Cell counts in the dilute samples were determined using a bright line hemacytometer cell counting chamber (Sigma Chemical Co., St. Louis, USA). For *S. aureus* measurement, 20 µL of each diluted sample (ranging from 1 to 10^8 CFU) was drop casted on the surface of the prepared immunosensor at room temperature. After 1h the immunosensors were gently rinsed with ultra-filtered water, and DPVs were conducted in a $[K_3Fe(CN)_6]/[K_4Fe(CN)_6]$ (5 mM/5 mM) solution in 10 mM PBS (pH 7.4).

The sensor's capability to detect *S. aureus* in biofilm was also assessed. Biofilm formation was carried out using a 96-well plate and cellulose sheets. Circular cellulose sheets were placed at the bottom of three wells and immersed in *S. aureus* solution. To study the effect of cellulose as a biofilm substrate, three additional wells without cellulose sheets were also filled with *S. aureus* solution while three wells containing only PBS served as the control group. The plates were then incubated at 38 °C for 24 h, after which light biofilm coatings became visible at the bottom of the wells. Afterward, the wells (with and without cellulose) were all carefully rinsed to remove free bacteria, then transferred to new wells filled with LB broth. These newly filled wells were incubated at 38 °C for another 48 h to allow the release of aureolysin into the solution. The detection of aureolysin was performed by dropping 30 µL of sample from each well onto the surface of fabricated electrodes. DPV measurements were conducted after incubating the electrode for 1 h, in a solution of $[K_3Fe(CN)_6/K_4Fe(CN)_6]$ (5 mM/5 mM) in 10 mM PBS (pH 7.4).

3. Results and Discussion

3.1. Electrochemical and Physicochemical Characterization of Au Nanospike Modified SPGE

Nanostructured surfaces were electrochemically prepared using fixed precursor concentrations of $HAuCl_4$ (6.8 mM) and 1 mM $Pb(CH_3COO)_2$ (1 mM).[30] To confirm successful growth of multidirectional Au nanospikes on the electrode, the surface morphology of Au nanospike-electrode was observed with SEM (**Figure 2A**). The treated surface appeared rough, uniformly covered with three-dimensional nanospikes with prismatic tapering ends and the top view image revealed nanospikes with a length of ≈500 nm and a base thickness dimension of ≈300 nm. In Figure 2, a comparison of bare SPGE (1) and Au-nanospike-SPGE (2) showed that the deposition of Au nanospikes causes a color change from yellow to brown, confirming successful modification.[47] Figure 2B displays the cyclic voltammetry profiles of SPGE before and after electrochemical treatment. The larger redox peaks for nanospike represent a higher electrochemical active surface area (ECSA) of the corresponding Au nanospike nanostructures compared to the bare Au electrode. The ECSA of both bare Au and Au nanospike electrodes was determined using cyclic voltammetry in 0.1 M H_2SO_4 solution.

The ECSA was calculated from the area under the reductive cathodic peak, which is proportional to the real surface area (ECSA = Q/390 µC.cm^{-2}) and reflects surface roughness.[48] This peak is attributed to the removal of oxide monolayer formed during the onward CV scan. As expected, the ECSA of the Au nanospike electrode (0.461 ± 0.032 cm^2) was significantly higher compared to that of bare Au electrode (0.060 ± 0.013 cm^2), as shown in Figure 2. Given the geometrical area of the bare Au electrode (0.126 cm^2), roughness factors (R_f, the ratio of ECSA to geometrical area) of 3.665 ± 0.258 for the Au nanospike electrode and 0.536 ± 0.106 for bare Au electrode were calculated, confirming the successful preparation of gold nanostructures.

The stability of the electrode surface was evaluated via DPV in $[K_3Fe(CN)_6]/[K_4Fe(CN)_6]$ over a period of 28 days. The stability was calculated as $(1-\Delta I/I_0) \times 100$ where $\Delta I/I_0 = (I_{dai(0)} - I_{day(n)})/I_{day(0)}$. The results depicted a slow decay in current stability over time with only 24% drop from the initial electrochemical activity after 3 weeks, reflecting the high stability of Au

© 2025 The Author(s). Advanced Sensor Research published by Wiley-VCH GmbH

27511219, 2025, 4, Downloaded from https://advanced.onlinelibrary.wiley.com/doi/10.1002/adsr.202400153, Wiley Online Library on [23/10/2025]. See the Terms and Conditions (https://onlinelibrary.wiley.com/terms-and-conditions) on Wiley Online Library for rules of use; OA articles are governed by the applicable Creative Commons License

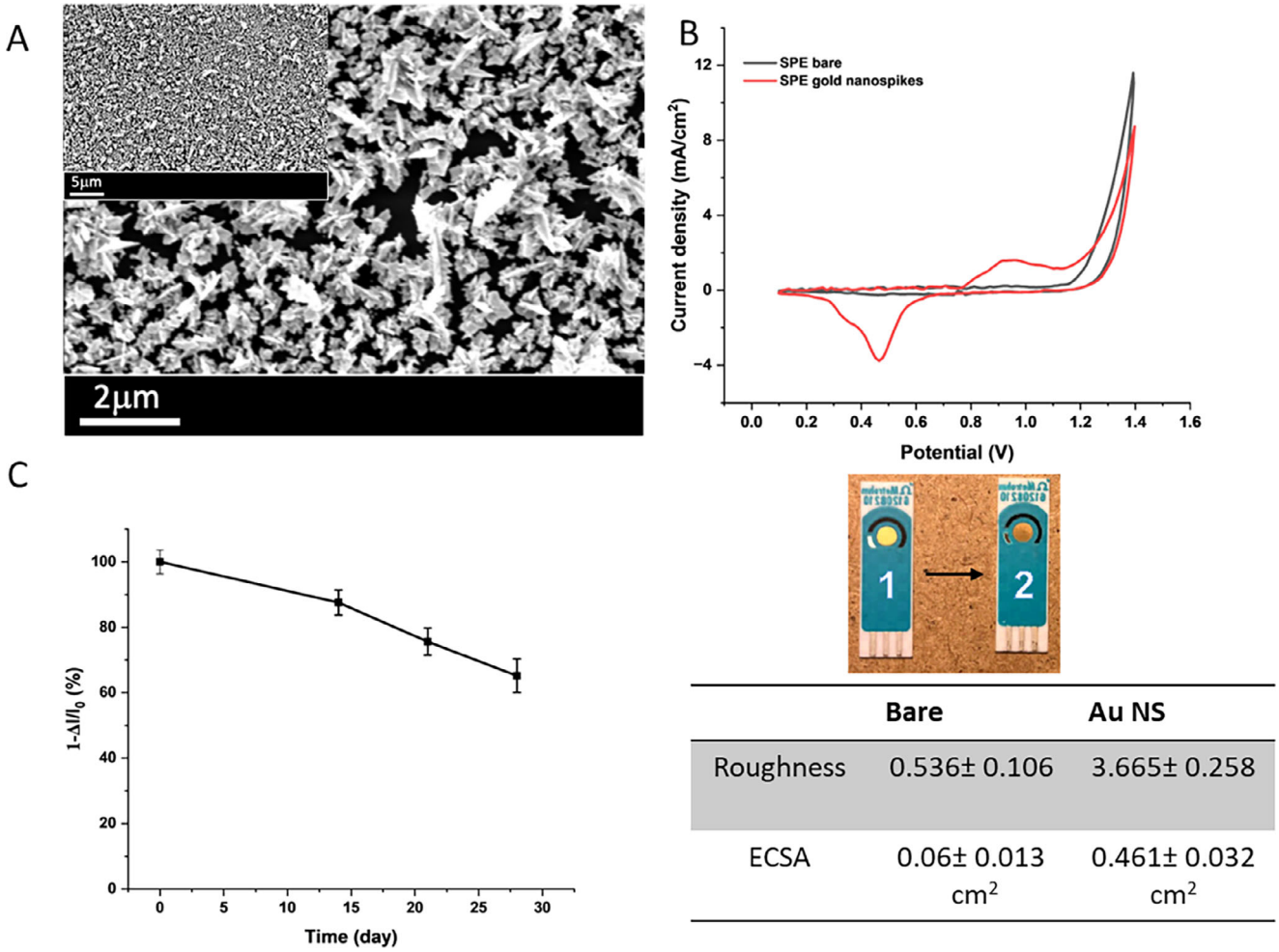

	Bare	Au NS
Roughness	0.536± 0.106	3.665± 0.258
ECSA	0.06± 0.013 cm^2	0.461± 0.032 cm^2

Figure 2. Photographs of SPGE and Aunanospike-SPGE A) Scanning electron micrographs of Aunanospike-SPGE at low and higher magnification. B) CVs obtained at 0.5 V s^{-1} in 0.1 M H_2SO_4 with (red) and without (black) Au nanospikes and associated ECSA and roughness. C) Stability of the Aunanospike-SPGE electrochemical signal for 28-day period.

nanospikes as a substrate structure for the electrochemical immunosensor (Figure 2C).

3.2. Characterization of BSA-Antibody-MUA-Au Nanospike-SPG Electrode

The fabrication of the immunosensor was characterized at each step using CV and DPV in $[K_3Fe(CN)_6]/[K_4Fe(CN)_6]$ as an electron transfer mediator. **Figure 3A** depicts the DPV curves for SPGE (blue), Aunanospike-SPGE (black), MUA-Aunanospike-SPGE (red), Antibody-MUA-Aunanospike-SPGE (green), BSA-Antibody-MUA-Aunanospike-SPGE (purple) and BSA-Antibody-MUA-Aunanospike-SPGE in presence of 10 pg. mL^{-1} of aureolysin (yellow). As shown in the DPV curves, the peak current density increased from 1.79 mA. cm^{-2} for the bare SPGE to 3.59 mA. cm^{-2} following the deposition of Au nanospike structures onto the SPGE, indicating an enhanced electron transfer between the solution and the electrode. Subsequently, following the formation of a self-assembly monolayer of 11-Mercaptoundecanoic acid on the surface of the Au nanospike, the peak current density significantly decreases to 1.14 mA. cm^{-2} due to the insulating behavior of the alkane chains. Subsequent immobilization of antibody and absorption of BSA led to further reduction of peak current density down to 915 μA. cm^{-2} for Ab modified electrode and 629 μA. cm^{-2} for BSA adsorbed electrode, likely caused by the insulating effects of Ab and BSA, which retard or block the electron transfer from the solution to the Au electrode.

In Figure 3B, a pair of well-defined redox peaks attributed to the $[Fe(CN)_6^{3-/4-}]$ redox couple was observed in the CV measurement, with the anodic and cathodic peak potential of 0.19 and 0.05 V, respectively, and a peak potential difference of 140 mV (blue curves). The results from the CV measurements were consistent with those from the DPV measurements, showing a decrease in the peak potential difference from 140 mV to 93 mV after modification, indicating increased electron transfer due to the high electrical conductivity and surface area of Au nanospikes.[49]

© 2025 The Author(s). Advanced Sensor Research published by Wiley-VCH GmbH

27511219, 2025, 4, Downloaded from https://advanced.onlinelibrary.wiley.com/doi/10.1002/adsr.202400153, Wiley Online Library on [23/10/2025]. See the Terms and Conditions (https://onlinelibrary.wiley.com/terms-and-conditions) on Wiley Online Library for rules of use; OA articles are governed by the applicable Creative Commons License

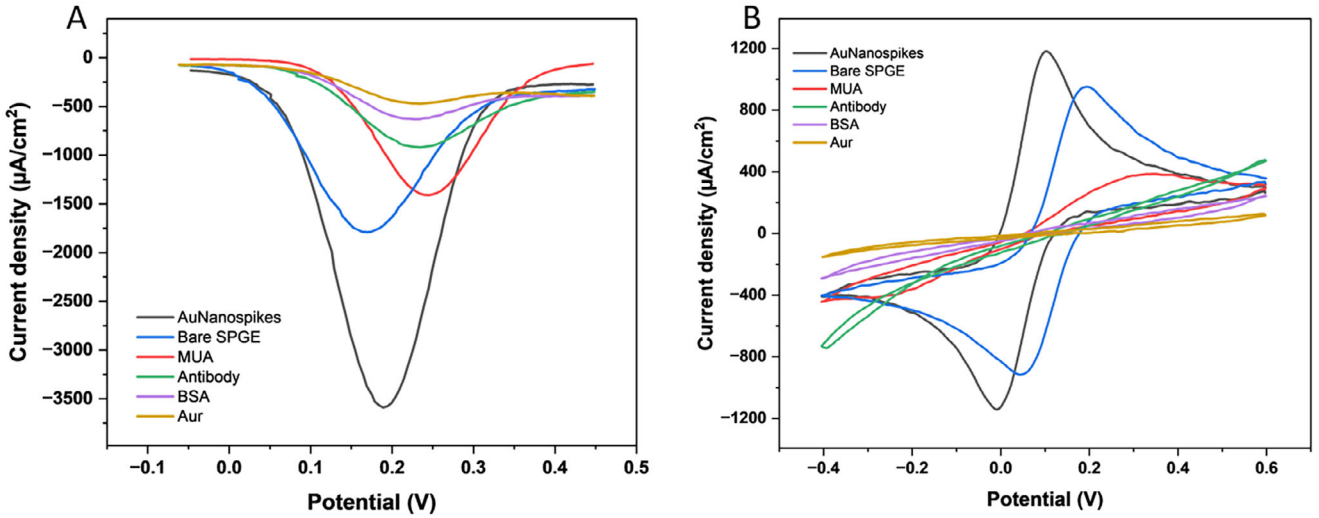

Figure 3. A) DPV- and B) CV- curves in 5 mM/5 mM $[K_3Fe(CN)_6]/[K_4Fe(CN)_6]$ as the redox medium for characterization of SPGE (blue), Aunanospike-SPGE (black), MUA-Aunanospike-SPGE (red), Antibody-MUA-Aunanospike-SPGE (green), BSA-Antibody-MUA-Aunanospike-SPGE (purple) and the immunosensor after incubating in 10 pg. mL^{-1} of aureolysin (yellow).

3.3. Differential Pulse Voltammograms for Aureolysin and *S. aureus* Detection

To evaluate the performance of the biosensor in terms of LOD and dynamic range, DPV experiments were conducted in PBS solution with increasing concentrations of aureolysin ranging from 1 to 100 pg. mL^{-1}. The change in current density, ΔJ, was calculated as the difference between the peak current density after incubation in Aur solution, J_{Aur}, and the baseline peak current density, J_{BSA}. As shown in **Figure 4A**, the peak current density decreases with increasing concentration of Aur, due to steric hindrance caused by the binding of Aur to the antibody immobilized on the electrode surface, which reduces electron transfer from the solution to the electrode. Figure 4B demonstrates

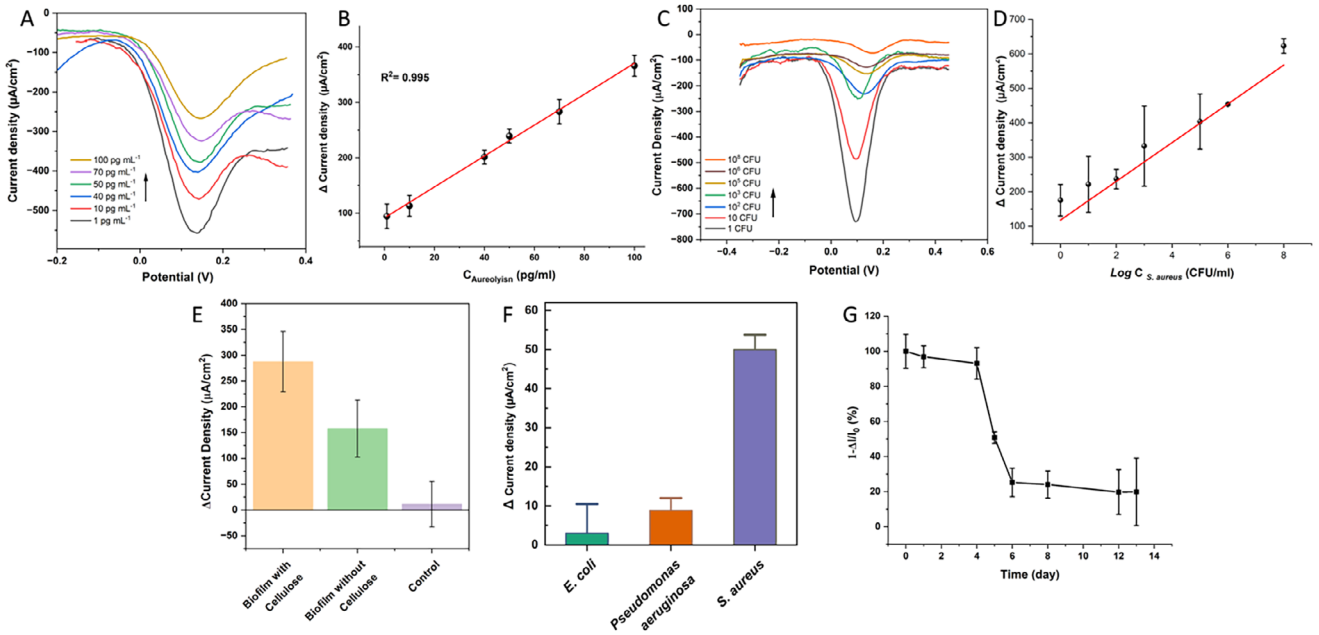

Figure 4. A) Differential pulse voltammograms of the SPGE immunosensor after exposing to Aur solutions with different concentrations of 1, 10, 40, 50, 70, and 100 pg·mL^{-1} (measured in 5 mM/5 mM $K_3Fe(CN)_6/K_4Fe(CN)_6$ solution in 10 mM PB (pH 7.4). B) Linear relationship between ΔJ and C_{auri}. C) Differential pulse voltammograms of the SPGE immunosensor after exposing to *S. aureus* solutions with different concentrations of 1, 10, 10^2, 10^3, 10^5, 10^6, and 10^8 CFU mL^{-1} (measured in 5 mM/5 mM $K_3Fe(CN)_6/K_4Fe(CN)_6$ solution in 10 mM PB (pH 7.4). D) Linear relationship between ΔJ and log (C *S. aureus*). E) Detection of *S. aureus* in biofilm. F) Selectivity of the immunosensor to *S. aureus* compared to *E. coli* and *P. aeruginosa*. G) Immunosensor stability over 13-day period.

© 2025 The Author(s). Advanced Sensor Research published by Wiley-VCH GmbH

27512219, 2025, 4, Downloaded from https://advanced.onlinelibrary.wiley.com/doi/10.1002/adsr.202400153, Wiley Online Library on [23/10/2025]. See the Terms and Conditions (https://onlinelibrary.wiley.com/terms-and-conditions) on Wiley Online Library for rules of use; OA articles are governed by the applicable Creative Commons License

Table 1. Comparison of different Electrochemical biosensors for *S. aureus* detection.

Working Electrode	Probe	Technique	Detection range	LOD	Interference	Sensor Stability	Refs.
SP* gold electrode	Pair of aptamers, sandwich-type	Signal-on chronoamperometry	1.9×10^2-2.5×10^4 CFU mL^{-1}	39 and 414 CFU mL^{-1}	*S. saprophyticus, S. typhimurium, L. monocytogenes, and E. coli*	–	[54]
MWCNT@CS/GCE*	Aptamer	DPV	10–10^7 CFU mL^{-1}	1 CFU mL^{-1}	*E. coli*, Sal. Typhimurium, B. subtilis, C. sporogeneses, S. pneumoniae	10 days	[15]
Gold electrode	dsDNA	DPV	60 to 6×10^7 CFU mL^{-1}	9 CFU mL^{-1}	E. faecium, L. monocytogenes, *P. aeruginosa*, *E. coli*, E. faecalis, S. enteritidis	-	[14]
ITO/PDDA/PSS/Au*	Anti-*S. aureus* antibody	EIS*	3×10^3–3×10^7 CFU mL^{-1}	10^3CFU mL^{-1}	*E. coli*, S. typhimurium, B. pumilus, K. pneumonia and B. subtilis	-	[21]
GCE/PDDA/PSS/GNR	Anti-*S. aureus* antibody	EIS	1.8×10^3 – 1.8×10^7 CFU mL^{-1}	10^2 CFU mL^{-1}	*E. coli, S. typhimurium, B. pumilus, B. subtilis*	14 days	[18]
GCE/AuNPs/MOF	anti-*S. aureus* Rosenbach tropina antibody	DPV	10–7.5×10^7 CFU mL^{-1}	6 CFU mL^{-1}	*E. coli, Bacillus cereus, and* Pseudomonas aeruginosa.	–	[20]
AuNP-modified SP electrode	Mouse monoclonal anti-MRSA* antibody	DPV and EIS	10–10^6 CFU mL^{-1}	13 CFU mL^{-1}	–	–	[17]
Aunanospike-SPGE	Aur Antibody	DPV	1-10^8 CFU mL^{-1}	2 CFU mL^{-1}	*E. coli, P. aeruginosa*	4 days	This work

SP: screen printed electrode; MWCNT: multiwalled carbon nanotubes; GCE: glassy carbon electrode; PDDA: Polydiallyldimethylammonium chloride; PSS: polystyrene sodium sulfonate; EIS: electrochemical impedance spectroscopy; MRSA: methicillin-resistant Staphylococcus aureus.

a linear relation between DPV current density (ΔJ) and C_{auri}, with a regression equation of Y = 2.791 C+ 91.610 (R^2 = 0.995). Three independent electrodes were used to acquire the calibration line. A low limit of detection of 5 pg. mL^{-1} (S/N = 3) was achieved, calculated by the IUPAC method (LOD = 3SD/S). This sensitivity is attributing to the high electrochemical activity and large surface area of the Au nanospikes.[50] The high surface area of the nanospikes provides a greater binding interface for the antibodies and facilitates the efficient transfer of electrons during the binding process.[51] This improves the sensitivity of the assay, enabling the detection of lower concentrations of the Aur. Experimental studies typically examine its immune interactions using concentrations ranging from 100 nM to 0.5 μM.[38,52] While direct clinical quantification remains limited, its documented abundance in *S. aureus* exoproteomes suggests biologically relevant levels during infection.[52] Our sensor achieves a detection limit of 5 pg·mL^{-1} (≈151 pM, based on its molecular weight of 33 kDa[39]), offering high sensitivity for detecting even trace amounts in clinical samples, thus enhancing its potential for early and accurate diagnosis.

Subsequent to Aur detection, DPV electrochemical characterization was conducted for S. aureus detection in bacterial cultures onto BSA-Antibody-MUA-Au nanospike-modified SPGE, with bacterial concentrations ranging from 1 to 10^8 CFU mL^{-1}. A blank response was measured after immersion and incubation in PBS without S. aureus. After 1h of incubation, the peak current decreased gradually as the bacterial concentration increased (Figure 4C). This decrease in peak current is the result of the formation of the Aur–Ab complex immobilized at the electrode surface, which inhibits electron transfer due to conformational change of electrode surface and steric hindrance. These findings confirm the applicability of the biosensor in detecting Aur secreted by *S. aureus* in complex environments. Figure 4D shows a strong linear relationship between *S. aureus* concentration and redox probe value with a LOD of 2 CFU mL^{-1} in bacterial culture (Y = 53.897log(C) + 157.06; R^2 = 0.974). The biosensor's applicability was further assessed for biofilm detection with BSA-Antibody-MUA-Au nanospike using DPV measurements after 1h of incubation. Experiments were conducted on biofilms formed on cellulose and polystyrene (no cellulose) surfaces, as well as in a PBS control solution. The biosensor response demonstrates successful detection of *S. aureus* in both biofilm types compared to the PBS control, confirming the release of aureolysin into the diluent solution over 48 h of incubation (Figure 4E). Notably, the biosensor detected a stronger aureolysin signal in biofilms formed on woven cellulose, as the cellulose sheet promoted greater biofilm growth, resulting in a higher bacterial load on its surface compared to the smooth polystyrene surface of a standard 96-well plate.

3.4. Cross-Reactivity and Stability Assay

A critical performance factor for biosensors is their specificity to the target of interest. To evaluate the selectivity test of the fabri-

© 2025 The Author(s). Advanced Sensor Research published by Wiley-VCH GmbH

27512219, 2025, 4, Downloaded from https://advanced.onlinelibrary.wiley.com/doi/10.1002/adsr.202400153, Wiley Online Library on [23/10/2025]. See the Terms and Conditions (https://onlinelibrary.wiley.com/terms-and-conditions) on Wiley Online Library for rules of use; OA articles are governed by the applicable Creative Commons License

cated biosensor, selectivity tests were carried out with other commonly encountered bacteria, namely *E. coli* and *P. aeruginosa*. The cross-reactivity testing was carried out on *P. aeruginosa* and *E. coli* on the *S. aureus* detection sensor because, like *S. aureus*, they are common in early PJI cases, where high-virulence pathogens prevail.[53] Cultured samples of these bacteria were diluted to a concentration of 10^5 CFU mL^{-1} and incubated for 1 h with the biosensor. The resulting changes in current density were measured using DPV under the same conditions applied for *S. aureus* samples. As shown in Figure 4F, minimal electrochemical signal changes were observed for *E. coli* and *P. aeruginosa*, likely due to nonspecific binding to the sensor surface. In contrast, the distinct current density changes observed for *S. aureus* confirm the biosensor's high specificity.

Sensor's stability was assessed by analyzing the DPV response of three prepared BSA-Antibody-MUA-Aunanospike-SPGE over a period of 13 days. During this time, the electrodes were stored in PBS at 4 °C. Figure 4G shows that after 1h of incubation, the biosensor retained 93% of its initial electrochemical signal after 4 days, which gradually decreased to 50% after 6 days.

A comparison of the performance of the present fabricated biosensor with other electrochemical biosensors for *S. aureus* detection is summarized in **Table 1**.

As shown in the table, this aureolysin biosensor achieves a lower limit of detection compared to other screen-printed electrode-based biosensors that detect whole bacteria.[54] Comparing to another study, an electrochemical immunosensor using self-assembled gold nanorods reported an LOD of 2.4×10^2 CFU mL^{-1}, whereas our immunosensor exhibits a significantly lower LOD.[18] Another example, Cai et al. utilized strand displacement amplification reaction in an electrochemical biosensor with a triple-helix molecular switch to achieve a LOD of 8 CFU mL^{-1} *S. aureus*.[55] Our proposed immunosensor, however, requires only 20 µL of sample without the need for any preparation or amplification step. Given its excellent analytical performance, simple and rapid preparation, the Au nanospike-based immunosensor holds great potential as a reliable and rapid tool for detecting *S. aureus* in bacterial culture samples, suggesting its suitability for clinical applications. Given its role in immune evasion and tissue invasion,[38] Aur quantification could complement existing diagnostic approaches, particularly in cases where traditional culture-based methods are inconclusive or time-consuming. Its detection in patient samples could enable identification of high-risk cases such as post-surgical infections, pneumonia, and periprosthetic joint infections.

4. Conclusion

In this work, a highly sensitive, label-free electrochemical immunosensor was developed for the detection of *S. aureus* using an anti-aureolysin antibody. The successful electrochemical deposition of Au nanospikes on SPGE provides a stable substrate with larger active surface area, facilitating a higher antibody immobilization and, consequently, enhanced sensitivity. The anti-aureolysin antibodies were covalently bound to self-assembly monolayer of MUA, serving as the biorecognition element. The biosensing platform demonstrated not only an excellent sensitivity, and great specificity toward *S. aureus* in bacterial culture and biofilm form but also a good stability over time. Our results indicated a linear detection range of 1–100 pg mL^{-1} and a LOD of 5 pg mL^{-1} for aureolysin in PBS buffer, as well as a detection range of 1–10^8 CFU mL^{-1} and an LOD of 2 CFU mL^{-1} for *S. aureus* in bacterial cultures. The combination of a low LOD and a wide detection range positions this immunosensor as a highly promising tool for rapid and reliable detection of *S. aureus*, with significant potential for clinical applications.

Acknowledgements

This research was funded by Merle, Natural Sciences and Engineering Research Council of Canada (NSERC) discovery, and Fonds de Recherche du Québec - Santé (FRQS) chercheur boursier J1.

Conflict of Interest

The authors declare no conflict of interest.

Author Contributions

Z.M. and G.M. performed conceptualization; Z.M. performed methodology; Z.M. performed validation; Z.M. performed formal analysis; G.M. acquired resources; Z.M., D.J., and G.C. performed data curation; Z.M. and Y.R. wrote the original draft; G.M. wrote the draft and reviewed it and also edited the original manuscript; G.M. performed supervision; G.M. acquired the funding acquisition All authors have read and agreed to the published version of the manuscript.

Data Availability Statement

The data that support the findings of this study are available from the corresponding author upon reasonable request.

Keywords

aureolysin, gold nanospikes, immunosensor, point-of-care diagnostic, *S. aureus*

Received: October 2, 2024
Revised: February 13, 2025
Published online: March 18, 2025

[1] G. Y. C. Cheung, J. S. Bae, M. Otto, *Virulence* **2021**, *12*, 547.
[2] C. L. Jenkins, H. D. Bean, *Pathogens* **2023**, *12*, 181.
[3] I. Fleurot, M. Aigle, R. Fleurot, C. Darrigo, J.-A. Hennekinne, A. Gruss, E. Borezée-Durant, A. Delacroix-Buchet, *Appl. Environ. Microbiol.* **2014**, *80*, 1815106.
[4] B. G. Botaro, C. S. Cortinhas, L. V. Março, J. F. G. Moreno, L. F. P. Silva, N. R. Benites, M. V. Santos, *J. Dairy Sci.* **2013**, *96*, 6955.
[5] A. Wieser, L. Schneider, J. Jung, S. Schubert, *Appl. Microbiol. Biotechnol.* **2012**, *93*, 965.
[6] F. McEachern, E. Harvey, G. Merle, *Biotechnol J. Sep.* **2020**, *15*, 2000140.
[7] Y.-D. Ma, K.-H. Li, Y.i-H. Chen, Y.-M. Lee, S.-T.a Chou, Y.-Y. Lai, P.o-C. Huang, H.-P. Ma, G.-B. Lee, *Lab Chip* **2019**, *19*, 3804.
[8] N. Bhardwaj, S. K. Bhardwaj, M. K. Nayak, J. Mehta, K.-H. Kim, A. Deep, *TrAC, Trends Anal. Chem.* **2017**, *97*, 120.

© 2025 The Author(s). Advanced Sensor Research published by Wiley-VCH GmbH

27511219, 2025, 4, Downloaded from https://advanced.onlinelibrary.wiley.com/doi/10.1002/adsr.202400153, Wiley Online Library on [23/10/2025]. See the Terms and Conditions (https://onlinelibrary.wiley.com/terms-and-conditions) on Wiley Online Library for rules of use; OA articles are governed by the applicable Creative Commons License

[9] Z. Huang, X. Yu, Q. Yang, Y. Zhao, W. Wu, *Front. Microbiol.* **2021**, *12*, 714265.
[10] R. Wang, L. Wang, J. Yan, D. Luan, Tao sun, J. Wu, X. Bian, *Talanta* **2021**, *226*, 122135.
[11] D. Han, Y. Yan, X. Bian, J. Wang, M. Zhao, X. Duan, L. Kong, W. Cheng, S. Ding, *Mikrochim. Acta* **2020**, *187*, 607.
[12] T. Wu, C. Wang, M. Wu, P. Wang, Q. Feng, *Food Chem.* **2022**, *382*, 132501.
[13] M. Simić, T. Kojić, M. Radovanović, G. M. Stojanović, *IEEE Sens. J.* **2020**, *20*, 12791.
[14] R. Cai, S. Zhang, L. Chen, M. Li, Y. Zhang, N. Zhou, *ACS Appl. Mater. Interfaces* **2021**, *13*, 4905.
[15] T. Wu, C. Wang, X. Han, Q. Feng, P. Wang, *Anal. Chim. Acta* **2022**, *1222*, 340179.
[16] S. Mousavi Nodoushan, N. Nasirizadeh, J. Amani, R. Halabian, A. A. Imani Fooladi, *Biosens. Bioelectron.* **2019**, *127*, 221.
[17] V. Q. Khue, T. Q. Huy, V. N. Phan, A. Tuan-Le, D. T. Thanh Le, M. Tonezzer, N. T. Hong Hanh, *Mater. Chem. Phys.* **2020**, *255*, 123562.
[18] E. Han, X. Li, Y. Zhang, M. Zhang, J. Cai, X. Zhang, *Anal. Biochem.* **2020**, *611*, 113982.
[19] H. Wang, Y. i. Xiu, Y. Chen, L. Sun, L. Yang, H. Chen, X. Niu, *RSC Adv.* **2019**, *9*, 16278.
[20] W.-C. Hu, J. Pang, S. Biswas, K. Wang, C. Wang, X.-H. Xia, *Anal. Chem.* **2021**, *93*, 8544.
[21] P. Gu, J. Huang, J. Yao, *Int. J. Electrochem. Sci.* **2021**, *16*, 211225.
[22] J. C. Soares, A. C. Soares, M. Popolin-Neto, F. V. Paulovich, O. N. Oliveira, L. H. C. Mattoso, *Sens. Actuators Rep.* **2022**, *4*, 100083.
[23] A. A. JVR, N. A. Hirst, P. A. Millner, *Clin. Microbiol. Rev.* **2014**, *27*, 631.
[24] A. J. Tande, R. Patel, *Clin. Microbiol. Rev.* **2014**, *27*, 302.
[25] Y. W. Hartati, A. A. Suryani, M. Agustina, S. Gaffar, A. Anggraeni, *Food Anal. Methods* **2019**, *12*, 2591.
[26] Z. Zhang, D. Vieira, J. E. Barralet, G. Merle, *2D Mater.* **2020**, *7*, 025044.
[27] H.-C. Chiang, Y. Wang, Q. Zhang, K. Levon, *Biosensor* **2019**, *9*, 50.
[28] L. C. Brazaca, A. H. Imamura, N. O. Gomes, M. B. Almeida, D. T. Scheidt, P. A. Raymundo-Pereira, O. N. Oliveira, B. C. Janegitz, S. A. S. Machado, E. Carrilho, *Anal. Bioanal. Chem.* **2022**, *414*, 5507.
[29] Y. Tian, H. Liu, G. Zhao, T. Tatsuma, *J. Phys. Chem. B* **2006**, *110*, 23478.
[30] B. Plowman, S. J. Ippolito, V. Bansal, Y. M. Sabri, A. P. O'Mullane, S. K. Bhargava, *Chem. Commun.* **2009**, 5039.
[31] A. Koushanpour, E. Harvey, G. Merle, *Sens. Diagn.* **2023**, *2*, 714.
[32] J. Perez, E. R. Gonzalez, H. M. Villullas, **1998**, *102*, 10931.
[33] A. Hamelin, M. J. Sottomayor, F. Silva, S.-C. Chang, M. J. Weaver, *J. Electroanal. Chem. Interfacial Electrochem.* **1990**, *295*, 291.
[34] I. Anshori, R. R. Althof, L. N. Rizalputri, E. Ariasena, M. Handayani, A. Pradana, M. R. Akbar, M. R. A. A. Syamsunarno, A. Purwidyantri, B. A. Prabowo, M. S. Annas, H. Munawar, B. Yuliarto, *Metals* **2022**, *12*, 2116.
[35] A. J. Barrett, J. F. Woessner, N. D. Rawlings, *Handbook of Proteolytic Enzymes*, Elsevier Academic Press, Amsterdam, Netherlands **2012**.
[36] A. Sabat, K. Kosowska, K. Poulsen, A. Kasprowicz, A. Sekowska, B. van den Burg, J. Travis, J. Potempa, *Infect. Immun.* **2000**, *68*, 973.
[37] M. R. Samar Solyman, A. Hanora, *Afr. J. Biotechnol.* **2021**, *20*, 77.
[38] A. J. Laarman, M. Ruyken, C. L. Malone, J. A. van Strijp, A. R. Horswill, S. H. Rooijakkers, *J. Immunol.* **2011**, *186*, 6445.
[39] S. R. M. UE, A. Rodríguez-Banqueri, T. Guevara, P. Czermak, E. Marcos, A. Vilcinskas, F. Xavier Gomis-Rüth, *Comput. Struct. Biotechnol. J* **2022**, *20*, 534.
[40] J. E. Cassat, N. D. Hammer, J. P. Campbell, M. A. Benson, D. S. Perrien, L. N. Mrak, M. S. Smeltzer, V. J. Torres, E. P. Skaar, *Cell Host Microbe* **2013**, *13*, 759.
[41] H. Elgharably, J. Claesen, N. Sangwan, M. Etiwy, P. Houghtaling, G. W. Procop, N. K. Shrestha, B. Griffin, J. L. Navia, L. G. Svensson, D. J. Wozniak, G. B. Pettersson, *JTCVS Open* **2024**
[42] M. Zdzalik, A. Y. Karim, K. Wolski, P. Buda, K. Wojcik, S. Brueggemann, P. Wojciechowski, S. Eick, A.-M. Calander, I.-M. Jonsson, M. Kubica, K. Polakowska, J. Miedzobrodzki, B. Wladyka, J. Potempa, G. Dubin, *FEMS Immunol. Med. Microbiol.* **2012**, *66*, 220.
[43] B. D. Gimza, J. K. Jackson, A. M. Frey, B. G. Budny, D. Chaput, D. N. Rizzo, L. N. Shaw, *mBio* **2021**, *12*, https://10.1128/mbio.03288-03220.
[44] S. L. Kolar, J. Antonio Ibarra, F. E. Rivera, J. M. Mootz, J. E. Davenport, S. M. Stevens, A. R. Horswill, L. N. Shaw, *MicrobiologyOpen* **2013**, *2*, 18.
[45] F. Rahman, I. Wushur, N. Malla, O. A. H. Åstrand, P. Rongved, J.-O. Winberg, I. Sylte, *Molecules* **2022**, *27*, 56.
[46] K. Tsikopoulos, G. Meroni, *Antibiotics* **2023**, *12*, 1485.
[47] H. Wan, Q. Sun, H. Li, F. Sun, N. Hu, P. Wang, *Sens. Actuators, B* **2015**, *209*, 336.
[48] L. Qian, R. Elmahdy, A. Raj Thiruppathi, A. Chen, *Analyst* **2021**, *146*, 4525.
[49] S. Liu, J. Liu, L. Wang, F. Zhao, *Bioelectrochemistry*. **2010**, *79*, 37.
[50] V. D. C. Rodrigues, C. H. Comin, J. C. Soares, A. C. Soares, M. E. Melendez, J. H. T. G. Fregnani, A. L. Carvalho, L. D. F. Costa, O. N. Oliveira, *ACS Appl. Mater. Interfaces* **2017**, *9*, 5885.
[51] F. Cui, Z. Zhou, H. Feng, H. S. Zhou, *ACS Appl Nano Mater.* **2020**, *3*, 357.
[52] S. R. Mendes, U. Eckhard, A. Rodríguez-Banqueri, T. Guevara, P. Czermak, E. Marcos, A. Vilcinskas, F. Xavier Gomis-Rüth, *Comput. Struct. Biotechnol. J* **2022**, *20*, 534.
[53] E. J. Weinstein, A. J. Stephens-Shields, C. W. Newcomb, R. Silibovsky, C. L. Nelson, J. A. O'Donnell, L. J. Glaser, E. Hsieh, J. S. Hanberg, J. P. Tate, K. M. Akgün, J. T. King, V. Lo Re, *JAMA Network Open* **2023**, *6*, 2340457.
[54] T. T.-Q. Nguyen, E. R. Kim, M. B. Gu, *Biosens. Bioelectron.* **2022**, *198*, 113835.
[55] R. F. Cai, Z. W. Zhang, H. H. Chen, Y. P. Tian, N. D. Zhou, *Sens. Actuators, B* **2021**, *326*, 128842.

© 2025 The Author(s). Advanced Sensor Research published by Wiley-VCH GmbH

27511219, 2025, 4, Downloaded from https://advanced.onlinelibrary.wiley.com/doi/10.1002/adsr.202400153, Wiley Online Library on [23/10/2025]. See the Terms and Conditions (https://onlinelibrary.wiley.com/terms-and-conditions) on Wiley Online Library for rules of use; OA articles are governed by the applicable Creative Commons License